

Quantum Analogs

Adam Green, Guillermo Acuna

agree019@ucr.edu, gacun002@ucr.edu

Department of Physics & Astronomy, University of California, Riverside, CA 92521

Abstract

Condense

In this experiment, we model the quantum mechanical wavefunction of the Hydrogen atom as a pressure wave inside a spherical cavity. The time evolution and spatial of these two waves, the wavefunction and pressure wave, are described by two different equations, the Schrödinger equation and wave equation respectively. However, under special conditions, the standing waves produced by these equations have striking similarity. For a spherical cavity, the angular dependence of the wave equation and Hydrogen atom are identical, and it is possible to generate standing waves inside the cavity which mimic the spherical harmonics of the Hydrogen atom. This allows us to determine ℓ values for each standing wave. However, the system contains a $(2\ell + 1)$ degeneracy. This degeneracy can be resolved by breaking the spherical symmetry of the cavity by introducing spacing rings. Once the symmetry is broken, a quantization axis is introduced and we can resolve the $m = 0$ and the $m = \pm 1$ peaks in the cavity.

Contents

1	Introduction	2
2	Experimental Procedure	4
2.1	Experiment Setup	4
2.2	Cavity Angles and Spherical Angles	4
2.3	Frequency Spectrum	5
2.4	Measuring Spherical Cavity Resonances with the Computer	6
2.5	Potential Problems	6
3	Results and Analysis	6
3.1	Determining Resonant Frequencies	6
3.2	Spectrum Response to Varying α	7
3.3	Determining ℓ Values for each Resonance	7
3.3.1	Comparison to Legender Polynomials	8
3.3.2	Comparison to Spherical Harmonics	8
3.4	$\ell = 1$ Degeneracy	9
3.5	Phase Measurements	11
4	Conclusion	11
4.1	Achievements	11

4.2	Future Improvements	12
5	Appendix	13
5.1	Cavity Angle and Polar Angle Relation	13
5.2	Amplitude and Polar Angle Measurement Tables	13
5.3	Legender Polynomial Comparisons	15
5.4	Spherical Harmonics	18
5.5	Polar Graphs with Broken Cavity Symmetry	20

1 Introduction

Often times in physics, the specific mathematical equations used to represent physical systems can become system-independent under special circumstances. In other words, the same equations can be used to describe very different systems. One intriguing example is a parallel between the Schrödinger equation and the wave equation. Both equations describe a sort of “wave.” In the Schrödinger equation, the “wave” is not a physical wave, but a probability wave. In the case of the wave equation, the wave is a physical pressure wave. Nonetheless, under special circumstances, these two equations can be modeled the same way.

In this experiment, we model the wavefunction of the Hydrogen atom with a physical pressure wave inside a hollow spherical cavity. This is possible because the conditions inside the spherical cavity mimic the conditions of a Hydrogen atom and the equations which describe the wavefunction and pressure wave have the same solution. We will begin by analyzing the solutions to both the Schrödinger equation and the wave equation.

The Schrödinger equation is used to describe the time-evolution of a quantum mechanical system and is given by:

$$i\hbar \frac{\partial \psi}{\partial t} = \left[-\frac{\hbar^2}{2m} \nabla^2 + V(\mathbf{r}, t) \right] \psi \quad (1)$$

where ψ is a complex wavefunction which has temporal and spatial dependence, $\psi = \psi(\mathbf{r}, t)$, and $V(\mathbf{r}, t)$ is a time and space dependent potential.

When the potential is time-independent, as in our case for the Coulomb potential $V = V(\mathbf{r})$, stationary states form in which the energy of the wavefunction remains constant and the Schrödinger equation reduces to:

$$E\psi = \left[-\frac{\hbar^2}{2m} \nabla^2 + V(\mathbf{r}) \right] \psi \quad (2)$$

For our case, the potential will be the Coulomb potential $V(r) = -e^2/r$. Taking advantage of spherical symmetry of the potential and spherical laplacian, we may rewrite the Schrödinger equation in spherical coordinates:

$$E\psi = -\frac{e^2}{r} + \frac{\hbar^2}{2m} \left[\frac{1}{r^2} \frac{\partial}{\partial r} r^2 \frac{\partial}{\partial r} + \frac{1}{r^2 \sin(\theta)} \frac{\partial}{\partial \theta} \sin(\theta) \frac{\partial}{\partial \theta} + \frac{1}{r^2 \sin^2(\theta)} \frac{\partial^2}{\partial \varphi^2} \right] \psi \quad (3)$$

where the first term is the Coulomb potential. We may solve Eqn. (3) with separation of variables, in which case the the solution admits the following form:

$$\psi(r, \theta, \varphi) = Y_\ell^m(\theta, \varphi) R(r) \quad (4)$$

The entire angular dependence of Eqn. (3) is contained in the spherical harmonics $Y_\ell^m(\theta, \varphi)$. Here, ℓ and m are the two quantum numbers representing angular momentum and magnetic spin respectively. Similarly, the entire radial dependence of Eqn. (3) is contained in $R(r)$.

The spherical harmonics $Y_\ell^m(\theta, \varphi)$ satisfy:

$$-\left[\frac{1}{\sin(\theta)}\frac{\partial}{\partial\theta}\sin(\theta)\frac{\partial}{\partial\theta} + \frac{1}{\sin^2(\theta)}\frac{\partial^2}{\partial\varphi^2}\right]Y_\ell^m = \ell(\ell+1)Y_\ell^m \quad (5)$$

and admit solutions which are proportional to the Legendre polynomials $P_\ell^m(\cos(\theta))$ and a complex exponential:

$$Y_\ell^m(\theta, \varphi) \propto P_\ell^m(\cos(\theta))e^{im\varphi} \quad (6)$$

The complex exponential however is not physical since it represents a quantum phase which is never observable.

The radial solution $R(r)$ satisfies:

$$-\frac{\hbar}{2m}\left[\frac{1}{r}\frac{\partial^2}{\partial r^2}r + \frac{\ell(\ell+1)}{r^2} + \frac{e^2}{r}\right]R(r) = E R(r) \quad (7)$$

We will now shift our attention to the spherical acoustic resonator which contains a pressure wave ρ whose time-evolution is described by the wave equation:

$$\frac{\partial^2\rho}{\partial t^2} = v^2 \nabla^2\rho \quad (8)$$

where v is the velocity of the wave, and the quantity $\rho = \rho(\mathbf{r}, t)$ represents the wave. To solve Eqn. (8), we assume the following functional form for the pressure wave:

$$\rho(\mathbf{r}, t) = P(\mathbf{r}) \cos(\omega t) \quad (9)$$

in which case, the wave equation reduces to the time-independent Helmholtz equation:

$$-\omega^2 P = \nabla^2 P \quad (10)$$

We pause here to draw a parallel between the Schrödinger equation, Eqn. (2), and the time-independent Helmholtz equation, Eqn. (10). Up to the addition of the the Coulomb potential in the Schrödinger equation, the two equations have the same differential form, and we expect similar solutions.

Proceeding in a similar fashion to the Schrödinger analysis, we take advantage of the spherical symmetry of the cavity and write Eqn. (10) in spherical coordinates:

$$\frac{\omega^2}{v^2}P = \left[-\frac{1}{r^2}\frac{\partial}{\partial r}r^2\frac{\partial}{\partial r} - \frac{1}{r^2\sin(\theta)}\frac{\partial}{\partial\theta}\sin(\theta)\frac{\partial}{\partial\theta} - \frac{1}{r^2\sin^2(\theta)}\frac{\partial^2}{\partial\varphi^2}\right]P \quad (11)$$

Again, up to the addition of the Coulomb potential, the spherical Helmholtz equation, Eqn. (11), has the same form as the spherical Schrödinger equation, Eqn. (3), so we expect similar behavior of the solutions.

We proceed in the same fashion and assume a separable solution to Eqn. (11) which takes the form:

$$P(r, \theta, \varphi) = Y_\ell^m(\theta, \varphi)F(r) \quad (12)$$

where the entire angular dependence of the pressure wave is contained in the spherical harmonics Y_ℓ^m just as the case with the Schrödinger equation. However, the radial component of the pressure wave obeys a slightly modified differential equation compared to the case of the Hydrogen atom:

$$\left[-\frac{\partial^2}{\partial r^2} - \frac{2}{r} \frac{\partial}{\partial r} + \frac{\ell(\ell+1)}{r^2} \right] F = \frac{\omega^2}{v^2} F \quad (13)$$

Since the Coulomb potential has no angular dependence, it does affect the angular solutions of either the Schrödinger equation or the Helmholtz equation and the angular dependence of both solutions are identical.

2 Experimental Procedure

2.1 Experiment Setup

This experiment utilized the *Quantum Analogs Controller* seen in Fig. 1a. The “Sine Wave Input” on the controller is connected to the signal generator and provides the frequency of the signal inside the cavity. The “Speaker Output” is connected to the speaker on the cavity. The microphone from the cavity is connected to the “Microphone Input” on the device. This reads the signal from the cavity into the controller. The “A/C Monitor” port is connected to channel 2 on our oscilloscope. This is the output of the microphone from inside the cavity. Finally, we connect the “Detector Output” on the controller to a multimeter set to read DC voltage. The controller converts the AC microphone signal to its envelope and outputs it as a DC signal to “Detector Output.” A full view of our lab bench can be used for reference in Fig. 1.

2.2 Cavity Angles and Spherical Angles

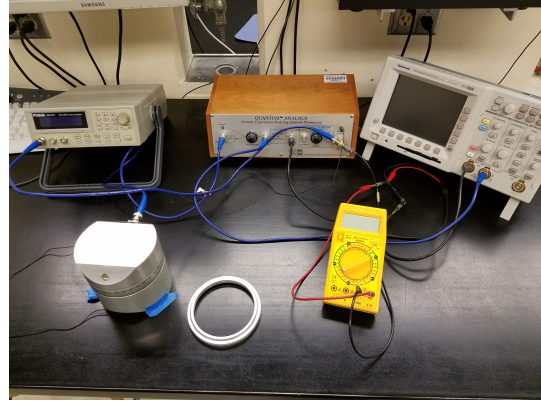
The main apparatus for this experiment is the spherical cavity. The microphone and speaker configuration inside the cavity is characterized by the *cavity angle* α . When spherical symmetry is present, the conversion from the cavity angle α to polar angle θ is:

$$\cos(\theta) = \frac{1}{2} \cos(\alpha) - \frac{1}{2} \quad (14)$$

In the appendix, Fig. 10 shows the relation between cosine of the polar angle θ and the cavity angle α . When the spherical symmetry is broken however, the system is quantized about the **z** axis perpendicular to the table, and the cavity angle is equal to the azimuthal angle φ .



(a) Quantum Analogs Controller

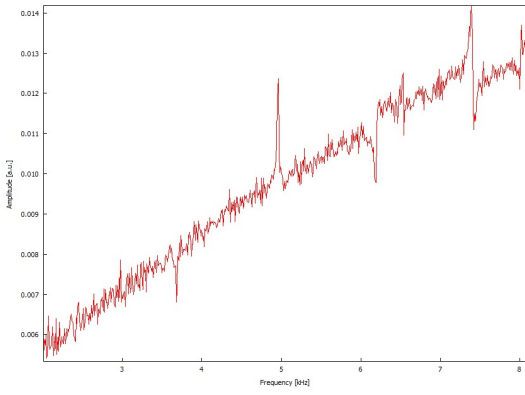


(b) Lab bench

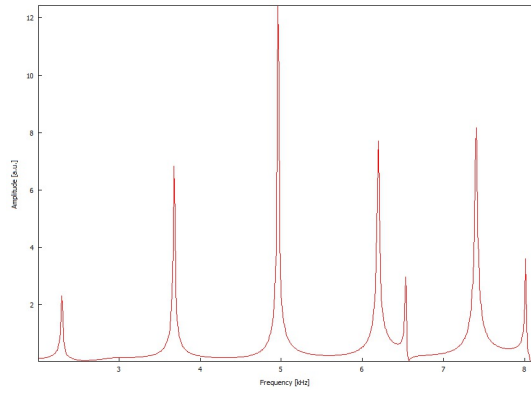
Figure 1: The *Quantum Analogs Controller* (a) and our table setup up (b)

2.3 Frequency Spectrum

Since the equations we are modeling are linear differential equations, we need to determine the frequency range where the cavity response is linear. measure the frequency spectrum over the entire frequency range, with the attenuation on the Quantum Analogs device set to its maximum setting, and focus our attention to the region where the spectrum increases linearly. We determine the linear regime of frequency response is between 2 kHz to 8.1 kHz. The linear regime of the frequency spectrum is shown in Fig. 2a. The large spikes indicate resonant frequencies. Once we determine the linear regime of the signal, we fine tune the attenuation and speaker amplitude to maximize signal and minimize cross-talk. The frequency spectrum for $\alpha = 180^\circ$ and 50% attenuation can be seen in Fig. 2b. The two smaller peaks at ≈ 6.5 kHz and 8 kHz are products of cross talk, and thus not resonances.



(a) Linear regime frequency spectrum with maximum attenuation



(b) Linear regime frequency spectrum with half attenuated signal

Figure 2: Fig (a) shows the linear regime of the frequency spectrum with maximum attenuation. Fig (b) shows that same frequency range with a half-attenuated signal.

2.4 Measuring Spherical Cavity Resonances with the Computer

In this section, we used the sound card in the computer to both generate and measure the resonances within the cavity. We set the attenuator to its highest value (10) to protect the sound card. The sound card output is connected to the Quantum Analogs *Sine Wave Input* and to channel 1 of the oscilloscope. The *AC Monitor* from the Quantum Analogs device is connected to the microphone input on the sound card and to channel 2 of the oscilloscope.

2.5 Potential Problems

One potential problem is the phenomena of *cross talk* when taking measurements with the computer. When the computer is being used to take measurements, it is simultaneously supplying the signal into the cavity. Cross talk occurs when the signal being sent into the cavity crosses into the line coming out of the cavity. Hence the input and output channels of the computer “talk” to each other.

One surefire way to eliminate cross talk is to simply use a higher quality sound card. If this is not an option, you will need to resort to adjusting the amplitude of the output, attenuation, and microphone sensitivities to minimize cross talk.

3 Results and Analysis

3.1 Determining Resonant Frequencies

Once we restricted our attention to the linear regime, see Fig. 2b, we began isolating the resonant frequencies using the oscilloscope. On the oscilloscope, a resonance will appear as an increase in the amplitude orders of magnitude larger than the characteristic scale of the signal. Near a resonance, we fine tune the frequency in increments of 1 Hz until the amplitude is maximized. It is important to note that denominations smaller than 1 Hz are not discernible on the oscilloscope due to the limited resolution of the screen. A table summarizing the resonant frequencies and their nodal angles is provided in Fig. 1. For a full summary of the acoustic amplitude vs polar angle measurements for all resonant frequencies, see tables 3-7 in the appendix. For the corresponding graphs of acoustic pressure versus polar angle, see figs. 11-15.

Resonant Frequency [Hz]	Uncertainty [Hz]	Nodal Angle(s) [Rad]	Uncertainty [Rad]
2291	1	1.91	1.65E-03
3679	1	2.09	1.51E-03
4962	1	1.64	1.72E-03
	1	2.53	4.24E-04
6202	1	2.00	1.73E-03
	1	2.65	1.41E-03
7409	1	1.64	1.74E-03
	1	2.09	1.51E-03
	1	2.77	6.27E-04

Table 1: Table of measured resonant frequencies, nodal angles, and associated uncertainties.

3.2 Spectrum Response to Varying α

Once we obtained the frequency spectrum in the linear regime of the signal, we varied α to observe how the spectrum changes as a function of cavity angle. Below are a series of measurements which show how the spectra changes as the cavity angle decreases from 40° to 0° .

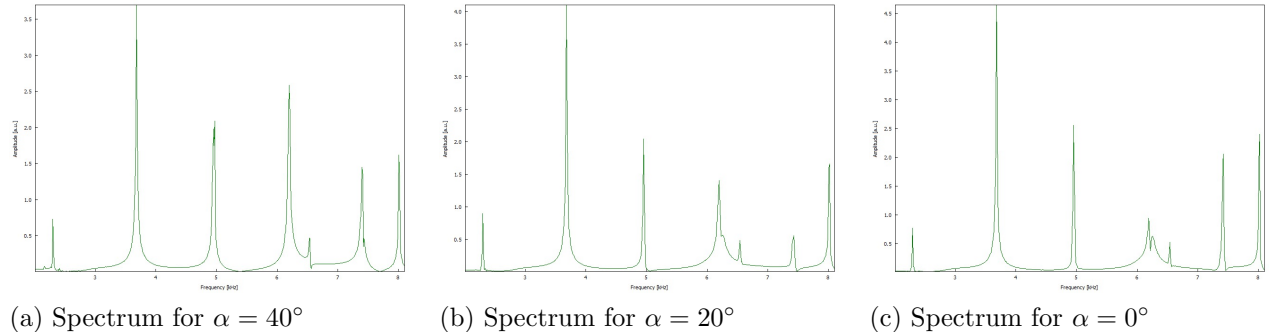


Figure 3: Graphs showing the spectrum as we vary the cavity angle α from 40° to 0° . We see very different behavior in the higher frequency resonances.

We can see that as the cavity angle approaches 0° , the resonance at ≈ 6 kHz starts large and drops off while the resonance at ≈ 7.5 kHz starts large, drops off, and then increases. This is due to the angular dependence of the spherical harmonics and specifically, the Legendre Polynomials. As the order of the polynomial increases, antinodes form closer and closer to $\cos(\theta) = 1$. In other words, the behavior of higher frequency resonances is more erratic near angles close to $\cos(\theta) = 1$, see the Legendre polynomials in figs. 16b, 17b, 18b, 19b and 20b in the appendix. So as we vary the cavity angle from 40° to 0° , some Legendre polynomials decrease while others increase.

3.3 Determining ℓ Values for each Resonance

Once we have isolated the resonant frequencies, we seek to determine what ℓ value they correspond to. We will present two ways to achieve this. First, we compare graphs of the acoustic amplitude vs $\cos(\theta)$ to the Legendre polynomials. Since the acoustic amplitude is the analog of the wavefunction, the shape of the graphs should match. Second, we compare the polar plots of acoustic amplitude vs polar angle to the spherical harmonics. This time, the polar plots should match the shapes of the spherical harmonics.

We begin by noting that for any quantum mechanical system, the wavefunction ψ is an inherently imaginary quantity. We can only ever observe real quantities however. To extract any observable quantity from the wavefunction, we must take its amplitude $|\psi|^2$. For the Hydrogen atom, the wavefunction is proportional to the spherical harmonics Y_m^ℓ and thus also proportional to the Legendre polynomials $P_\ell(\cos(\theta))$. So, the graphs of acoustic amplitude vs $\cos(\theta)$ should match the magnitude of the Legendre polynomials from the amplitude of the wavefunction $|P_\ell(\cos(\theta))|^2$. Similarly, polar plots of acoustic amplitude should match the real component of the spherical harmonics.

3.3.1 Comparison to Legender Polynomials

In this section, we determine the ℓ value of the 7409 Hz resonance by comparison to a Legendre polynomial. We present below, a single comparison of acoustic pressure and the corresponding Legendre polynomial. The rest of the comparisons may be found in figs. 16-20 in the Appendix.

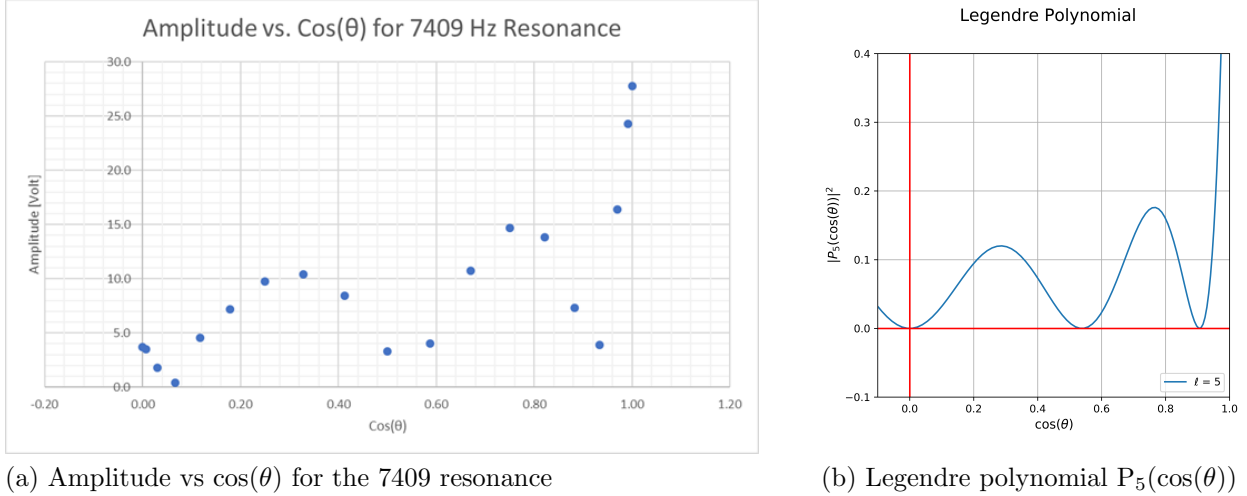


Figure 4: Qualitative comparison of the 7409 Hz resonance and the $\ell = 5$ Legendre polynomial.

The distinguishing features of Fig. 4a are the starting location at $\cos(\theta) = 0$ and the number of nodes. Since the amplitude starts relatively close to zero, and has 3 nodes total, a qualitative comparison suggests that the 7409 Hz resonance corresponds to $\ell = 5$.

L	Legendre	Measured	Difference
1	0.00	0.333	0.333
2	0.58	0.496	0.081
3	0.00	0.069	0.069
	0.77	0.819	0.044
4	0.34	0.416	0.076
	0.86	0.882	0.020
	0.00	0.069	0.069
5	0.54	0.496	0.042
	0.91	0.932	0.026

Table 2: Table of numerically calculated zeros of the Legendre polynomials and the measured zeros.

we set the angle on the cavity to $\alpha = 180^\circ$ and record the acoustic amplitude using the “Measure wavefunction” button on the computer. We then decrease α from 180° to 0° in increments of $\alpha = 10^\circ$.

Once we obtained the polar amplitude plots, we can simply compare them qualitatively to the real component of the spherical harmonics. Fig. 5 below shows one such comparison. The

3.3.2 Comparison to Spherical Harmonics

To make a comparison to the spherical harmonics, we began mapping out how the acoustic amplitude varies as a function of cavity angle at each resonance. To begin,

To make a comparison to the spherical harmonics, we began mapping out how the acoustic amplitude varies as a function of cavity angle at each resonance. To begin,

remaining polar acoustic amplitude plots can be seen in Fig. 21 and their corresponding spherical harmonics in Fig. 22 in the Appendix. From this qualitative comparison, it is possible to determine the ℓ value for each resonance.

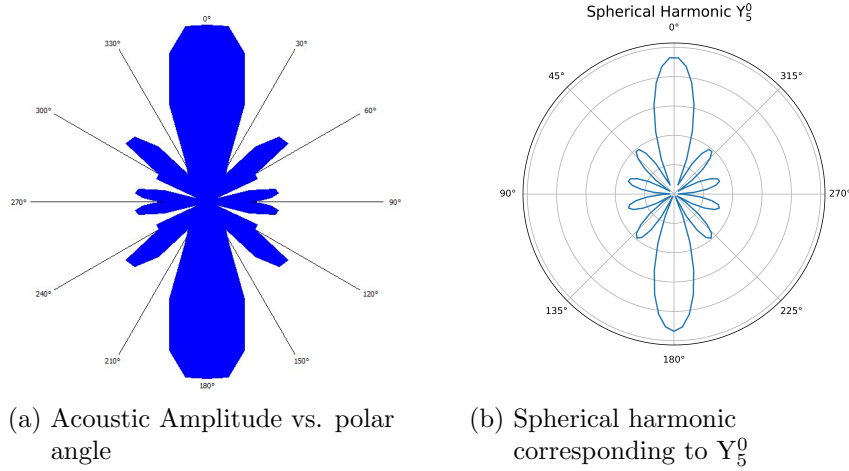


Figure 5: A comparison between the acoustic amplitude as a function of cavity angle and the corresponding spherical harmonic for the 7409 Hz resonance.

3.4 $\ell = 1$ Degeneracy

Recall that a quantum system with angular momentum ℓ has a $(2\ell+1)$ degeneracy of states. It is possible to resolve these degeneracies by breaking the spherical symmetry of the cavity. We achieve this by introducing spacing rings into the cavity, simulating a magnetic field which introduces a quantization axis into the system. This symmetry-breaking process is visualized in Fig. 6, where we can observe the peak splitting as the spacing is increased. The two peaks that emerge are the $m = 0$ and $m = \pm 1$, which is still degenerate.

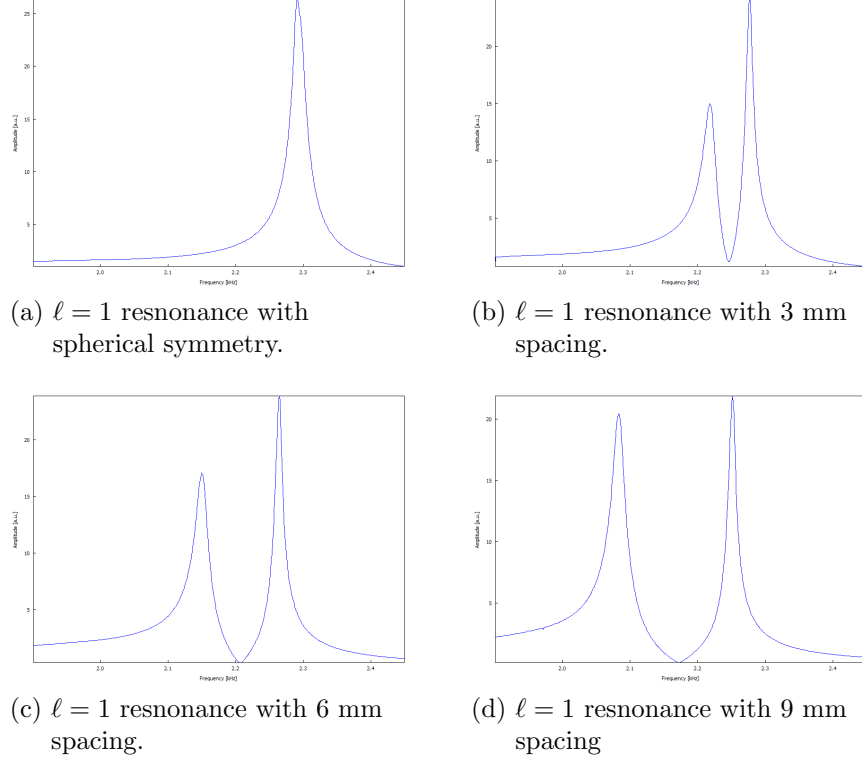


Figure 6: We can see as we break the spherical symmetry by introducing spacer rings to the cavity, the degeneracy in the $\ell = 1$ resonance is lifted and we can resolve the $m = 0$ and $m = \pm 1$ peaks.

We may further investigate by examining polar plots of the amplitude to determine the magnetic quantum number m . Fig. 7 shows the $\theta = 0$ projection of acoustic pressure vs. azimuthal angle φ for a cavity with the maximal separation of 9 mm. Azimuthal amplitude graphs for the 3 mm and 6 mm spacing rings can be seen in Fig. 23 and Fig. 24 in the appendix.

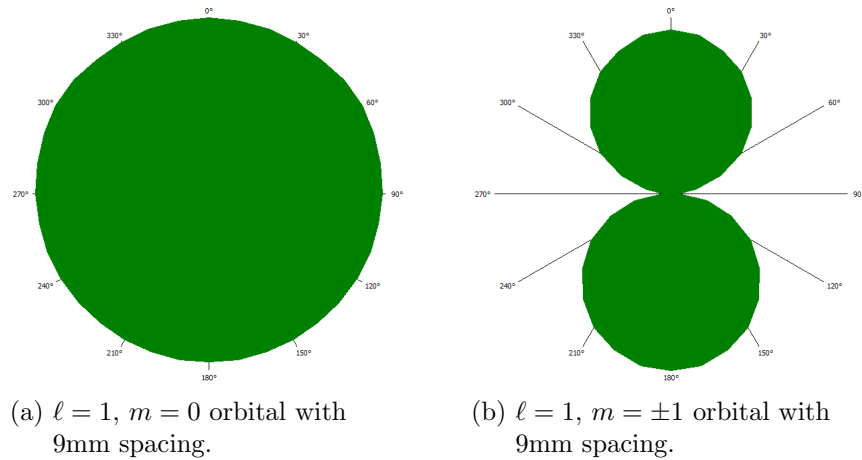


Figure 7: Projections of acoustic amplitude vs azimuthal angle (φ) onto the $\theta = 0$ plane. Angle markings indicate the azimuthal angle φ .

By comparing these graphs to the spherical harmonics, we can resolve the $\ell = 1$ state into $m = 0$ and $m = \pm 1$. The $m = \pm 1$ states are still degenerate because they are symmetric under rotations in the azimuthal angle φ . This can be seen in the $\varphi = 0$ projections of the spherical harmonics in Fig. 8. The projection of Fig. 8a onto the $\theta = 0$ plane exactly recovers Fig. 7a. Similarly, the projection of Fig. 8b onto the $\theta = 0$ plane exactly recovers Fig. 7b up to rotations in ϕ

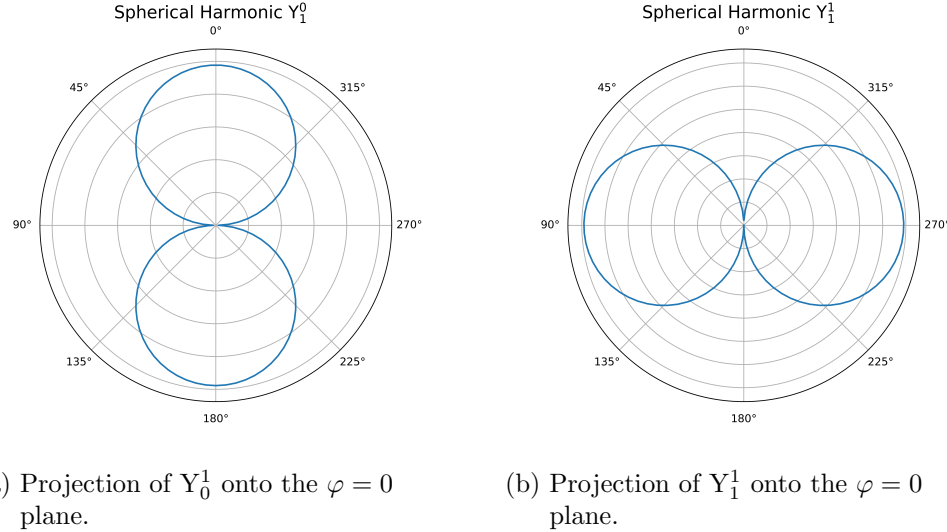


Figure 8: Projections of the spherical harmonics onto the $\varphi = 0$ plane. Angle markings indicate polar angle θ .

3.5 Phase Measurements

TO DO

m	Hemisphere	3mm [Deg]	Error [Deg]	6mm [Deg]	Error [Deg]	9mm [Deg]	Error [Deg]
0	Lower	87.28	5	95.91	2	178.6	1
0	Upper	-92.17	2	-86.49	1	-8.032	1
1	Lower	-83.29	2	-65.32	1	9.685	1
1	Upper	-52.08	2	-63.81	1	14.81	1

Figure 9: Table of measured phases for top and bottom hemispheres for all spacer rings

4 Conclusion

4.1 Achievements

In this experiment, we successfully modeled the angular dependence of the Hydrogen wavefunction with a standing pressure wave inside a spherical cavity. Plots of acoustic pressure versus cavity angle match those of the Legendre polynomials. Similarly, polar plots of acoustic pressure versus polar angle match the spherical harmonics. Further, we simulated the Zeeman effect and

achieved partial energy level splitting in the $\ell = 1$ state. We were only able to resolve the $m = 0$ and $m = \pm 1$ states however because $m = \pm 1$ is symmetric in the azimuthal angle.

4.2 Future Improvements

Throughout this experiment, the microphone was extremely sensitive to any noise and even vibrations in the room, chairs moving, the lab bench being bumped, doors closing, etc... One improvement to this experiment is to perform it in an isolated room on a sand table which dampens vibrations from the environment.

5 Appendix

All numerical calculations were written and performed in Python.

5.1 Cavity Angle and Polar Angle Relation

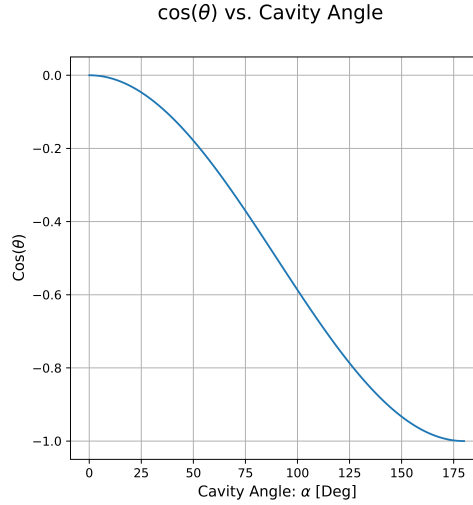


Figure 10: Relation between $\cos(\theta)$ and cavity angle α when spherical symmetry is present

5.2 Amplitude and Polar Angle Measurement Tables

For clarity, instead of plotting $\cos(\theta)$ we plot $|\cos(\theta)|$ since cosine is symmetric about $\theta = 0$.

Resonant frequency: 2291 Hz					
Alpha [Deg]	Alpha Error [Deg]	Theta [Rad]	Theta Error [Rad]	Amplitude [Volts]	Error [Volts]
0.00E+00	1.00E-01	1.57E+00	1.75E-03	5.69E-02	1.00E-03
1.00E+01	1.00E-01	1.58E+00	1.75E-03	6.01E-02	1.00E-03
2.00E+01	1.00E-01	1.60E+00	1.74E-03	5.87E-02	1.00E-03
3.00E+01	1.00E-01	1.64E+00	1.74E-03	5.91E-02	1.00E-03
4.00E+01	1.00E-01	1.69E+00	1.73E-03	4.26E-02	1.00E-03
5.00E+01	1.00E-01	1.75E+00	1.72E-03	4.16E-02	1.00E-03
6.00E+01	1.00E-01	1.82E+00	1.69E-03	3.40E-02	1.00E-03
7.00E+01	1.00E-01	1.91E+00	1.65E-03	3.29E-02	1.00E-03
8.00E+01	1.00E-01	2.00E+00	1.59E-03	4.76E-02	1.00E-03
9.00E+01	1.00E-01	2.09E+00	1.51E-03	5.01E-02	1.00E-03
1.00E+02	1.00E-01	2.20E+00	1.41E-03	6.19E-02	1.00E-03
1.10E+02	1.00E-01	2.31E+00	1.29E-03	6.54E-02	1.00E-03
1.20E+02	1.00E-01	2.42E+00	1.15E-03	7.86E-02	1.00E-03
1.30E+02	1.00E-01	2.53E+00	9.94E-04	8.59E-02	1.00E-03
1.40E+02	1.00E-01	2.65E+00	8.18E-04	8.75E-02	1.00E-03
1.50E+02	1.00E-01	2.77E+00	6.27E-04	9.91E-02	1.00E-03
1.60E+02	1.00E-01	2.90E+00	4.24E-04	9.91E-02	1.00E-03
1.70E+02	1.00E-01	3.02E+00	2.13E-04	1.03E-01	1.00E-03
1.80E+02	1.00E-01	3.14E+00	1.41E-06	1.03E-01	1.00E-03

Table 3: Data table for resonant frequency 2291 Hz.

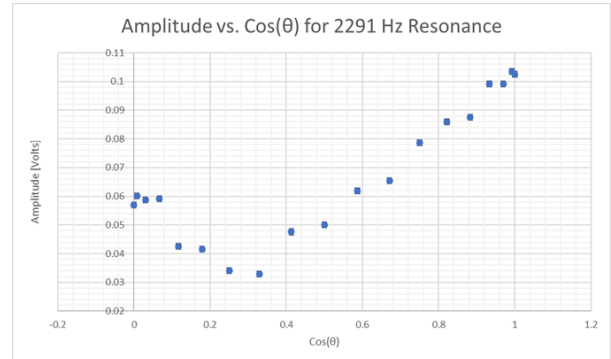


Figure 11: Graph of table 3. We can clearly see a single node at $\theta = 1.91$ radians.

Resonant frequency: 3679 Hz					
Alpha [Deg]	Alpha Error [Deg]	Theta [Rad]	Theta Error [Rad]	Amplitude [Volts]	Error [Volts]
0.00E+00	1.00E-01	1.57E+00	1.75E-03	1.91E+01	1.00E-03
1.00E+01	1.00E-01	1.58E+00	1.75E-03	1.90E+01	1.00E-03
2.00E+01	1.00E-01	1.60E+00	1.74E-03	1.91E+01	1.00E-03
3.00E+01	1.00E-01	1.64E+00	1.74E-03	1.90E+01	1.00E-03
4.00E+01	1.00E-01	1.69E+00	1.73E-03	1.89E+01	1.00E-03
5.00E+01	1.00E-01	1.75E+00	1.72E-03	1.77E+01	1.00E-03
6.00E+01	1.00E-01	1.82E+00	1.69E-03	1.08E+01	1.00E-03
7.00E+01	1.00E-01	1.91E+00	1.65E-03	9.76E+00	1.00E-03
8.00E+01	1.00E-01	2.00E+00	1.59E-03	4.59E+00	1.00E-03
9.00E+01	1.00E-01	2.09E+00	1.51E-03	1.33E+00	1.00E-03
1.00E+02	1.00E-01	2.20E+00	1.41E-03	4.17E+00	1.00E-03
1.10E+02	1.00E-01	2.31E+00	1.29E-03	6.21E+00	1.00E-03
1.20E+02	1.00E-01	2.42E+00	1.15E-03	9.55E+00	1.00E-03
1.30E+02	1.00E-01	2.53E+00	9.94E-04	1.53E+01	1.00E-03
1.40E+02	1.00E-01	2.65E+00	8.18E-04	1.48E+01	1.00E-03
1.50E+02	1.00E-01	2.77E+00	6.27E-04	1.58E+01	1.00E-03
1.60E+02	1.00E-01	2.90E+00	4.24E-04	1.56E+01	1.00E-03
1.70E+02	1.00E-01	3.02E+00	2.13E-04	1.57E+01	1.00E-03
1.80E+02	1.00E-01	3.14E+00	1.41E-06	1.59E+01	1.00E-03

Table 4: Table showing amplitude vs polar angle for 3679 Hz resonance.

Resonant frequency: 4962 Hz					
Alpha [Deg]	Alpha Error [Deg]	Theta [Rad]	Theta Error [Rad]	Amplitude [Volts]	Error [Volts]
0.00E+00	1.00E-01	1.57E+00	1.75E-03	2.33E+01	1.00E-03
1.00E+01	1.00E-01	1.58E+00	1.75E-03	2.33E+01	1.00E-03
2.00E+01	1.00E-01	1.60E+00	1.74E-03	2.31E+01	1.00E-03
3.00E+01	1.00E-01	1.64E+00	1.74E-03	2.21E+01	1.00E-03
4.00E+01	1.00E-01	1.69E+00	1.73E-03	1.59E+01	1.00E-03
5.00E+01	1.00E-01	1.75E+00	1.72E-03	5.42E+00	1.00E-04
6.00E+01	1.00E-01	1.82E+00	1.69E-03	7.52E+00	1.00E-03
7.00E+01	1.00E-01	1.91E+00	1.65E-03	1.66E+01	1.00E-03
8.00E+01	1.00E-01	2.00E+00	1.59E-03	2.13E+01	1.00E-03
9.00E+01	1.00E-01	2.09E+00	1.51E-03	2.30E+01	1.00E-03
1.00E+02	1.00E-01	2.20E+00	1.41E-03	2.32E+01	1.00E-03
1.10E+02	1.00E-01	2.31E+00	1.29E-03	2.20E+01	1.00E-03
1.20E+02	1.00E-01	2.42E+00	1.15E-03	1.67E+01	1.00E-03
1.30E+02	1.00E-01	2.53E+00	9.94E-04	1.25E+01	1.00E-03
1.40E+02	1.00E-01	2.65E+00	8.18E-04	6.63E+00	1.00E-04
1.50E+02	1.00E-01	2.77E+00	6.27E-04	2.16E+00	1.00E-04
1.60E+02	1.00E-01	2.90E+00	4.24E-04	2.11E+00	1.00E-04
1.70E+02	1.00E-01	3.02E+00	2.13E-04	7.41E+00	1.00E-03
1.80E+02	1.00E-01	3.14E+00	1.41E-06	6.31E+00	2.00E-04

Table 5: Table showing amplitude vs polar angle for 4926 Hz resonance.

Resonant frequency: 6202 Hz					
Alpha [Deg]	Alpha Error [Deg]	Theta [Rad]	Theta Error [Rad]	Amplitude [Volts]	Error [Volts]
0.00E+00	1.00E-01	1.57E+00	1.75E-03	2.58E+01	1.00E-03
1.00E+01	1.00E-01	1.58E+00	1.75E-03	2.50E+01	1.00E-03
2.00E+01	1.00E-01	1.60E+00	1.74E-03	1.73E+01	1.00E-03
3.00E+01	1.00E-01	1.64E+00	1.74E-03	7.45E+00	1.00E-03
4.00E+01	1.00E-01	1.69E+00	1.73E-03	3.00E+00	1.00E-03
5.00E+01	1.00E-01	1.75E+00	1.72E-03	1.04E+01	1.00E-03
6.00E+01	1.00E-01	1.82E+00	1.69E-03	1.43E+01	1.00E-03
7.00E+01	1.00E-01	1.91E+00	1.65E-03	1.56E+01	1.00E-03
8.00E+01	1.00E-01	2.00E+00	1.59E-03	1.40E+01	1.00E-03
9.00E+01	1.00E-01	2.09E+00	1.51E-03	8.83E+00	1.00E-03
1.00E+02	1.00E-01	2.20E+00	1.41E-03	3.23E+00	1.00E-03
1.10E+02	1.00E-01	2.31E+00	1.29E-03	6.93E+00	1.00E-03
1.20E+02	1.00E-01	2.42E+00	1.15E-03	8.62E+00	1.00E-03
1.30E+02	1.00E-01	2.53E+00	9.94E-04	9.34E+00	1.00E-03
1.40E+02	1.00E-01	2.65E+00	8.18E-04	8.66E+00	1.00E-03
1.50E+02	1.00E-01	2.77E+00	6.27E-04	7.59E+00	1.00E-03
1.60E+02	1.00E-01	2.90E+00	4.24E-04	6.48E+00	1.00E-03
1.70E+02	1.00E-01	3.02E+00	2.13E-04	4.86E+00	1.00E-03
1.80E+02	1.00E-01	3.14E+00	1.41E-06	4.41E+00	1.00E-03

Table 6: Table showing amplitude vs polar angle for 6202 Hz resonance.

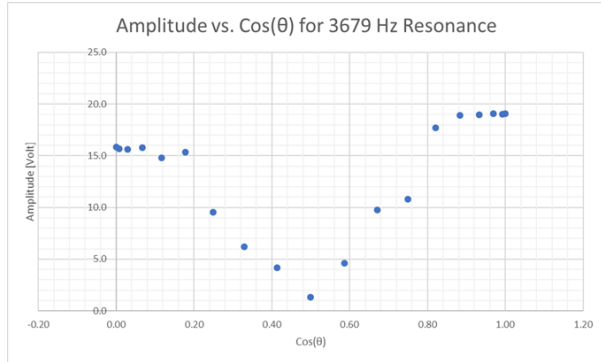


Figure 12: Graph of table 4. We can clearly see a single node at $\theta = 2.09$ radians.

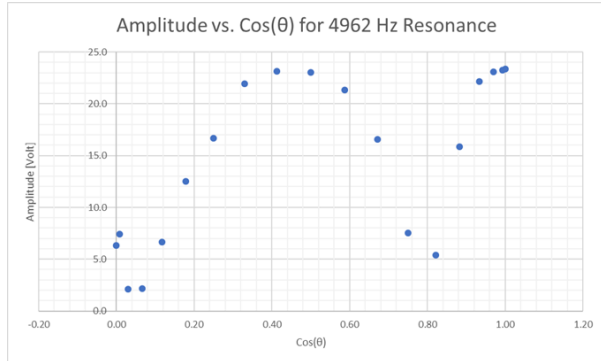


Figure 13: Graph of table 5. We can clearly see a single node at $\theta = \pi$ radians.

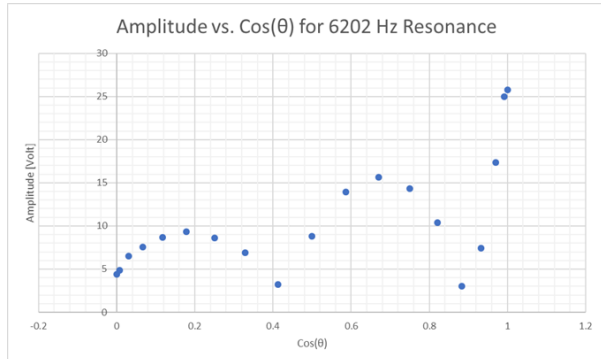


Figure 14: Graph of table 6. We can clearly see a single node at $\theta = \pi$ radians.

Resonant frequency: 7409 Hz					
Alpha [Deg]	Alpha Error [Deg]	Theta [Rad]	Theta Error [Rad]	Amplitude [Volts]	Error [Volts]
0.00E+00	1.00E-01	1.57E+00	1.75E-03	2.78E+01	1.00E-03
1.00E+01	1.00E-01	1.58E+00	1.75E-03	2.43E+01	1.00E-03
2.00E+01	1.00E-01	1.60E+00	1.74E-03	1.64E+01	1.00E-03
3.00E+01	1.00E-01	1.64E+00	1.74E-03	3.90E+00	1.00E-03
4.00E+01	1.00E-01	1.69E+00	1.73E-03	7.31E+00	1.00E-03
5.00E+01	1.00E-01	1.75E+00	1.72E-03	1.38E+01	1.00E-03
6.00E+01	1.00E-01	1.82E+00	1.69E-03	1.47E+01	1.00E-03
7.00E+01	1.00E-01	1.91E+00	1.65E-03	1.08E+01	1.00E-03
8.00E+01	1.00E-01	2.00E+00	1.59E-03	4.03E+00	1.00E-03
9.00E+01	1.00E-01	2.09E+00	1.51E-03	3.31E+00	1.00E-04
1.00E+02	1.00E-01	2.20E+00	1.41E-03	8.45E+00	1.00E-03
1.10E+02	1.00E-01	2.31E+00	1.29E-03	1.04E+01	1.00E-03
1.20E+02	1.00E-01	2.42E+00	1.15E-03	9.76E+00	1.00E-03
1.30E+02	1.00E-01	2.53E+00	9.94E-04	7.17E+00	1.00E-03
1.40E+02	1.00E-01	2.65E+00	8.18E-04	4.59E+00	1.00E-03
1.50E+02	1.00E-01	2.77E+00	6.27E-04	4.41E-01	1.00E-04
1.60E+02	1.00E-01	2.90E+00	4.24E-04	1.81E+00	1.00E-04
1.70E+02	1.00E-01	3.02E+00	2.13E-04	3.48E+00	1.00E-03
1.80E+02	1.00E-01	3.14E+00	1.41E-06	3.72E+00	1.00E-03

Table 7: Table showing amplitude vs polar angle for 7409 Hz resonance.

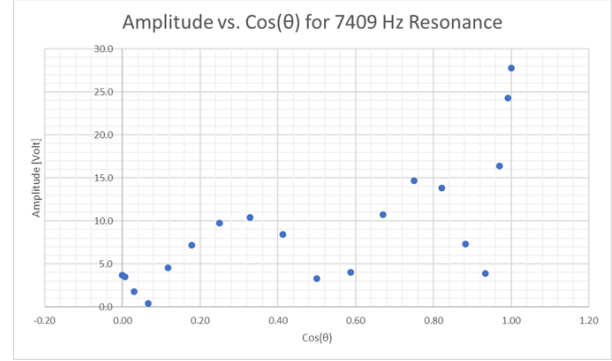
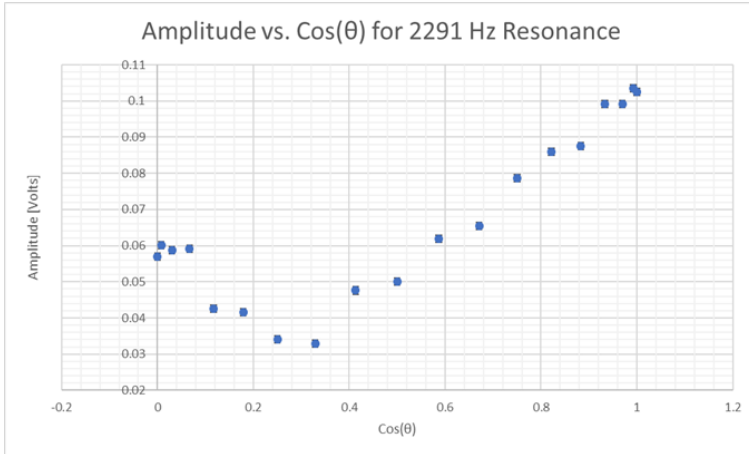
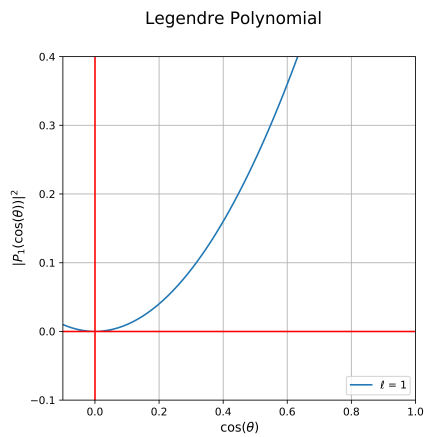


Figure 15: Graph of table 7. We can clearly see a single node at $\theta = \pi$ radians.

5.3 Legender Polynomial Comparisons

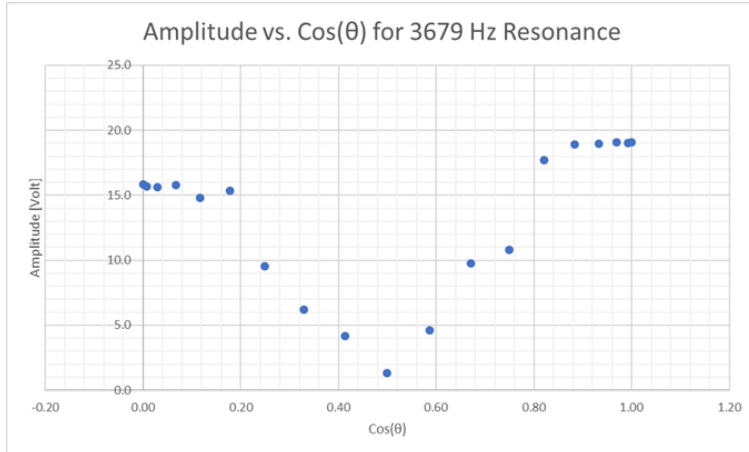


(a) Measured acoustic amplitude plotted against $\cos(\theta)$ for the 2291 Hz resonance

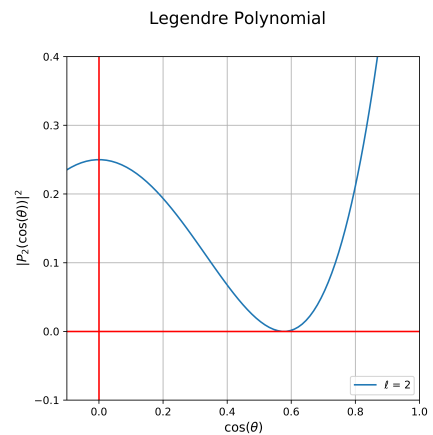


(b) Legendre polynomial $|P_1|^2$

Figure 16: Comparison of the measured data and the $\ell = 1$ Legendre polynomial for the 2291 Hz resonance.

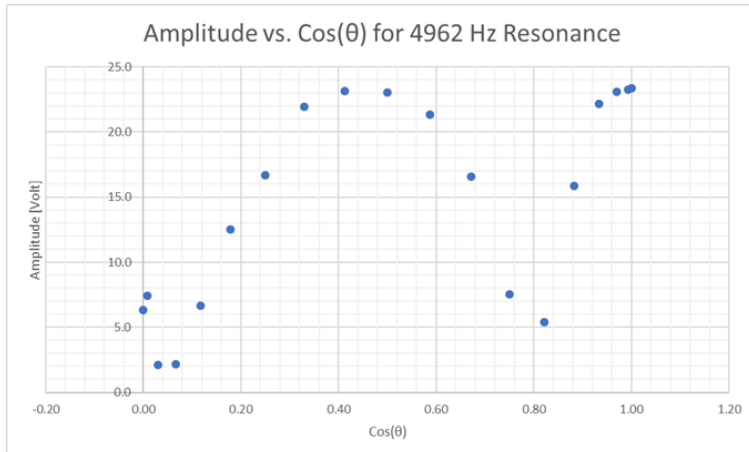


(a) Measured acoustic amplitude plotted against $\cos(\theta)$ for the 3679 Hz resonance

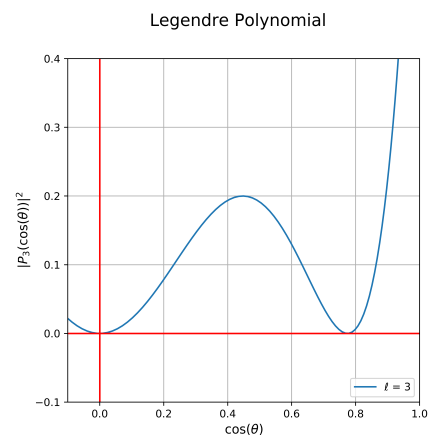


(b) Legendre polynomial $|P_2|^2$

Figure 17: Comparison of the measured data and the $\ell = 2$ Legendre polynomial for the 3679 Hz resonance.

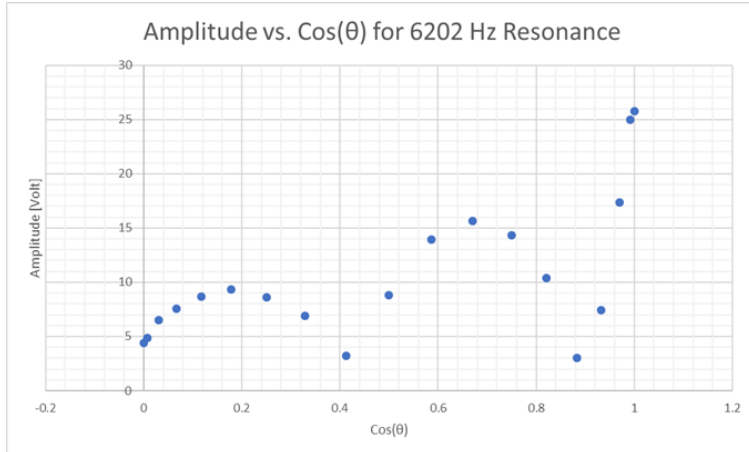


(a) Measured acoustic amplitude plotted against $\cos(\theta)$ for the 4962 Hz resonance

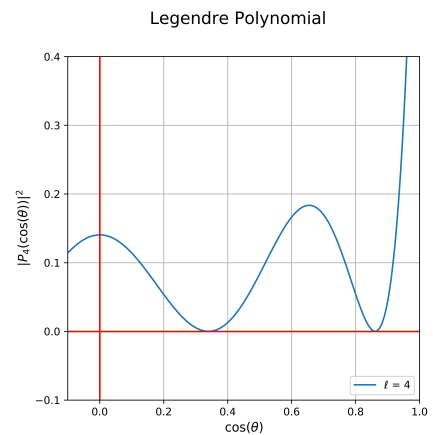


(b) Legendre polynomial $|P_3|^2$

Figure 18: Comparison of the measured data and the $\ell = 3$ Legendre polynomial for the 4962 Hz resonance.

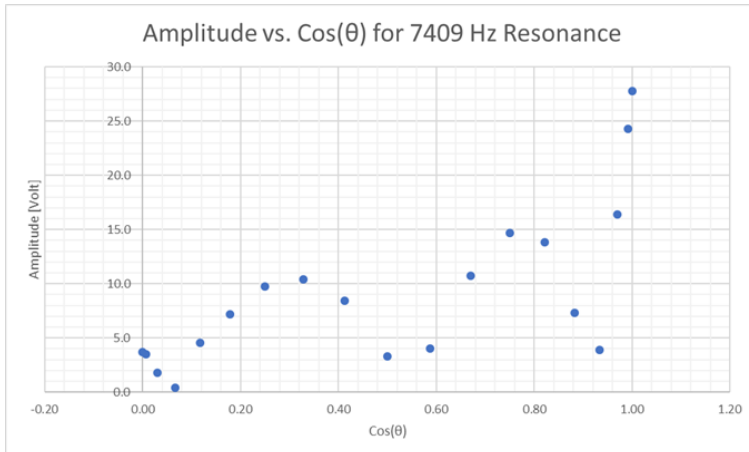


(a) Measured acoustic amplitude plotted against $\cos(\theta)$ for the 6202 Hz resonance

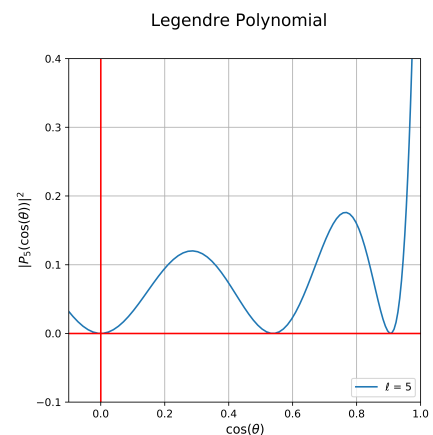


(b) Legendre polynomial $|P_4|^2$

Figure 19: Comparison of the measured data and the $\ell = 4$ Legendre polynomial for the 6202 Hz resonance.



(a) Measured acoustic amplitude plotted against $\cos(\theta)$ for the 7409 Hz resonance



(b) Legendre polynomial $|P_5|^2$

Figure 20: Comparison of the measured data and the $\ell = 5$ Legendre polynomial for the 7409 Hz resonance.

5.4 Spherical Harmonics

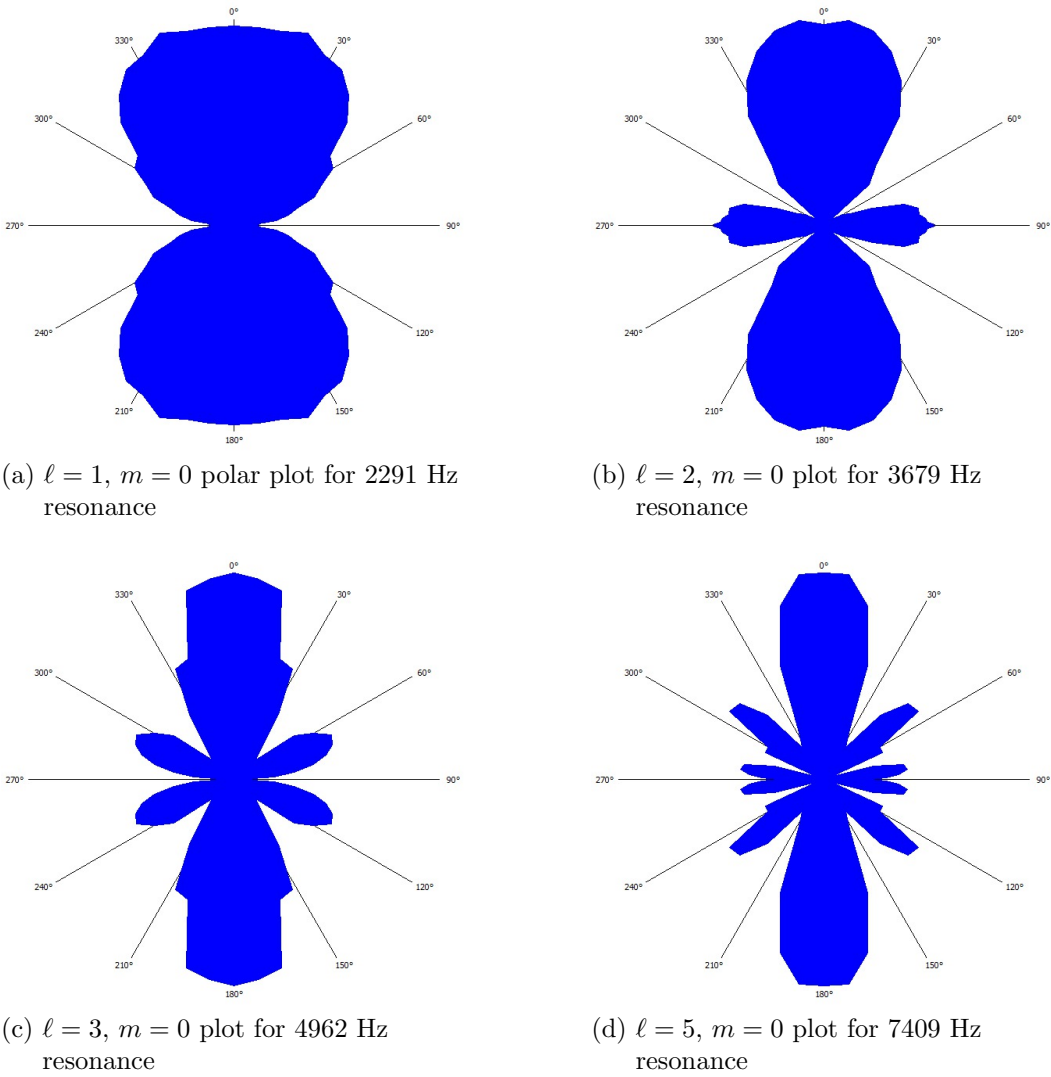
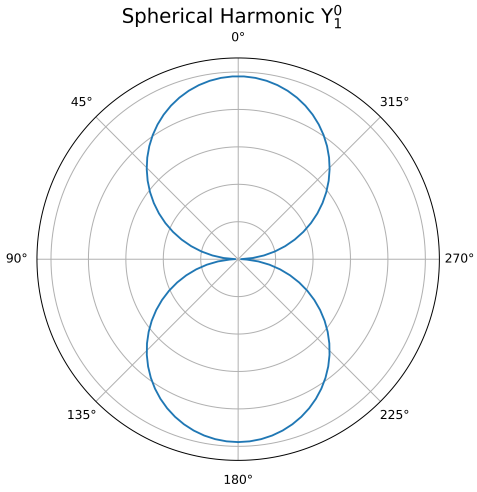
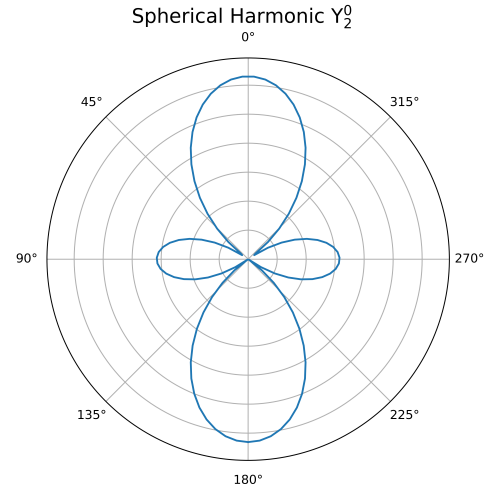


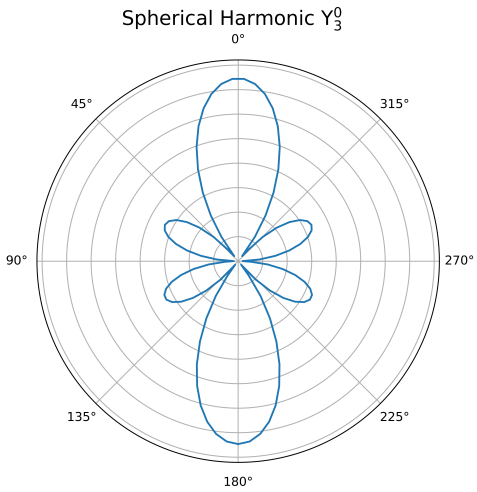
Figure 21: Acoustic amplitude vs polar angle (θ) with azimuthal angle $\varphi = 0$ for 4 resonant frequencies. Comparing these to the spherical harmonics in Fig. 22, it is possible to determine the angular momentum quantum number ℓ for each resonance.



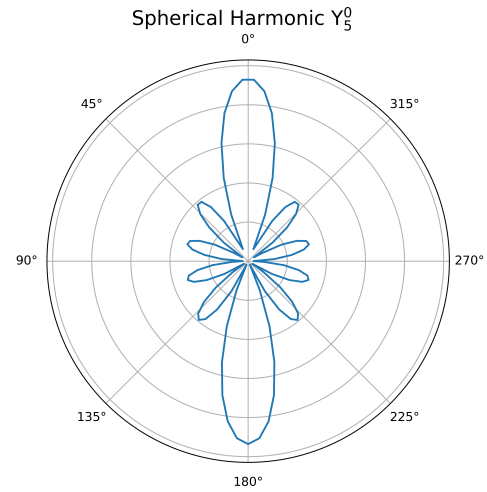
(a) Spherical harmonic for $\ell = 1, m = 0$



(b) Spherical harmonic for $\ell = 2, m = 0$



(c) Spherical harmonic for $\ell = 3, m = 0$



(d) Spherical harmonic for $\ell = 5, m = 1$

Figure 22: Projections of the spherical harmonics Y_m^ℓ onto the $\varphi = 0$ plane. Angle markings indicate polar angle θ .

5.5 Polar Graphs with Broken Cavity Symmetry

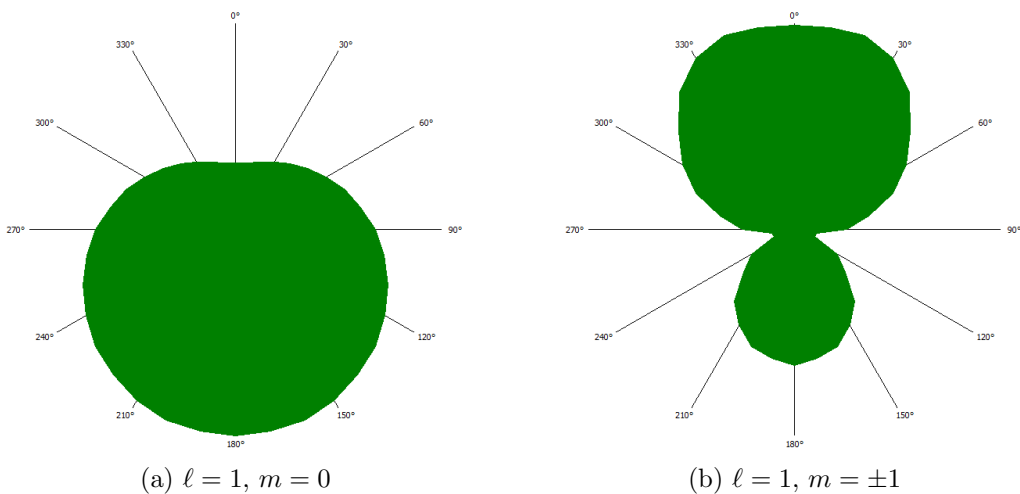


Figure 23: Amplitude versus polar angle θ for the $\ell = 1$ resonance with 3mm Spacing

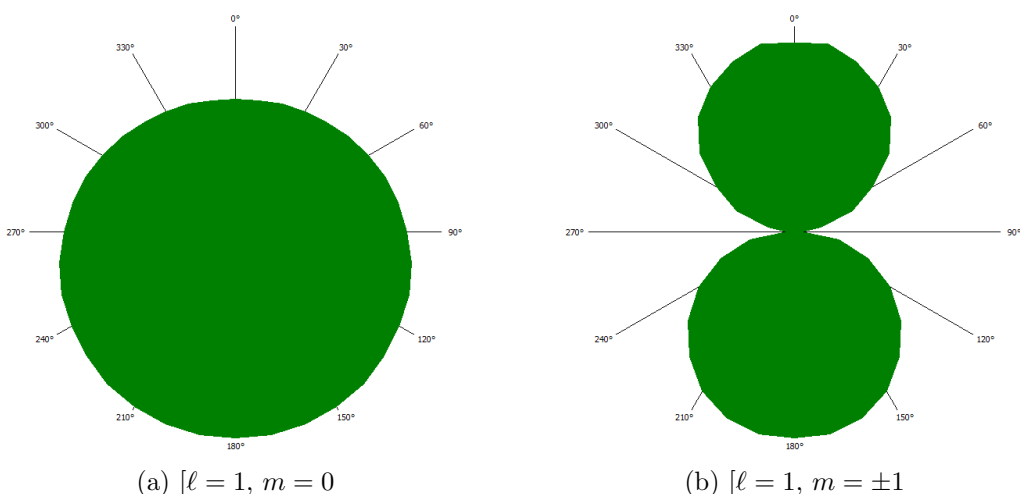


Figure 24: Amplitude versus polar angle θ for the $\ell = 1$ resonance with 6mm Spacing

We can see that as the cavity separation is increased, simulating a stronger magnetic field, the shapes of the orbitals becomes more symmetric.

References

- [1] D. H. McIntyre, *Quantum Mechanics*. Pearson, 2012.
- [2] W. Boyce and R. DiPrima, *Elementary Differential Equations and Boundary Value Problems, 10th Edition*. Laurie Rosatone, 2012.